RSC Advances

PAPER

View Article Online
View Journal | View Issue

Open Access Article. Published on 18 February 2019. Downloaded on 1/26/2026 8:40:42 AM.
This article is licensed under a Creative Commons Attribution-NonCommercial 3.0 Unported Licence.

Check for updates

Cite this: *RSC Adv.*, 2019, **9**, 5995

Efficient dehydrogenation of a formic acid–ammonium formate mixture over Au_3Pd_1 catalyst†

Xiao-Tong Guo, Juan Zhang, Jian-Chao Chi, Zhi-Hui Li, Yu-Chen Liu, Xin-Ru Liu and Shu-Yong Zhang *

Received 20th November 2018
Accepted 14th February 2019

DOI: 10.1039/c8ra09534e

rsc.li/rsc-advances

A series of AuPd/C catalysts were prepared and tested for the first time for active and stable dehydrogenation of a formic acid–ammonium formate (FA–AF) mixture. The catalysts with different Au-to-Pd molar ratios were prepared using a facile simultaneous reduction method and characterized using transmission electron microscopy (TEM), high-resolution TEM, energy dispersive X-ray spectroscopy, X-ray diffraction, and X-ray photoelectron spectroscopy. It was found that the catalytic activity and stability of the Au_3Pd_1/C catalyst was the best. The initial turnover frequency for the dehydrogenation of the FA–AF mixture over the Au_3Pd_1/C catalyst can reach 407.5 h^{-1} at 365 K. The reaction order with respect to FA and AF is 0.25 and 0.55, respectively. The apparent activation energy of dehydrogenation is 23.3 ± 1.3 kJ mol^{-1}. The catalytic activity of the Au_3Pd_1/C catalyst remains *ca.* 88.0% after 4 runs, which is much better than the single Pd/C catalyst. The mechanism for the dehydrogenation is also discussed.

1. Introduction

Due to its environmental friendliness and renewability, hydrogen has received extensive attention as the most promising energy carrier.[1–5] However, the commercial application of hydrogen is still facing great challenges due to the lack of credible technologies for the efficient generation, safe storage and transportation of gaseous hydrogen. Compared to the traditional physical methods, chemical methods for the storage and release of hydrogen are usually less expensive, more efficient, easier to handle and much safer.[6–8] However, the dehydrogenation or conversion of hydrocarbon, methanol, or ethanol can be only achieved at high temperature with several harmful by-products hard to separate.[9,10] Recently, owing to its high hydrogen content of 4.4 wt%, low toxicity, safe storage, easy transportation and efficient direct dehydrogenation, formic acid (FA) has been regarded as an ideal hydrogen storage medium.[11–15] FA can decompose through two competing paths: dehydrogenation/decarboxylation (1) and dehydration/decarbonylation (2).[15,16]

$$HCOOH(l) \rightarrow CO_2(g) + H_2(g) \quad (1)$$

$$HCOOH(l) \rightarrow CO(g) + H_2O(l) \quad (2)$$

CO produced through reaction (2) can poison fuel cell catalysts.[17,18]

Pd, one of the most active catalysts for the dehydrogenation of FA, also suffers from poisoning due to the trace amount of CO generated through reaction (2).[19] For single Pd catalysts,[20–27] only a few catalysts show suitable activity and stability. Recently, Au nanoparticles (NPs) or nanoclusters were found to be active for the dehydrogenation of FA.[28–34] The weak adsorption of CO and H atoms on the Au surface is beneficial to the catalyst performance.[35–39] Although some Au catalysts displayed excellent performances in both activity and stability, most of them showed relatively low turnover frequencies (TOFs) and high activation energies. To improve the activity of Au catalysts and the poison tolerance of Pd catalysts, the combination of Pd and Au may be a possible choice. In fact, a number of AuPd catalysts have been reported with improved catalytic performances.[40–45] The other way to improve the activity and stability of catalysts is using new fuel systems with low acidity, high formate anion concentration and catalyst enhancement agents such as formic acid–sodium formate (FA–SF) mixture or formic acid–ammonium formate (FA–AF) mixture.[46–50]

In a previous work, we found that the dehydrogenation performance of FA–AF mixture was even better than FA–SF mixture. The Pd/C catalyst exhibited superior catalytic activity towards FA–AF system with an initial TOF of 7959 h^{-1} at 323 K. However, the stability the Pd/C catalyst needs further improvement.[51]

In this work, we intend to take advantage of the improved stability of AuPd/C catalyst and the higher activity and catalysis enhancement of FA–AF mixture to develop a new system with improved dehydrogenation performance. A series of AuPd/C catalysts with different Au-to-Pd molar ratios were prepared and tested. The reaction order, apparent activation energy and the dehydrogenation mechanism are also discussed.

School of Chemistry and Chemical Engineering, Shandong University, Jinan 250100, P. R. China. E-mail: syzhang@sdu.edu.cn; Tel: +86-531-88365456

† Electronic supplementary information (ESI) available. See DOI: 10.1039/c8ra09534e

Open Access Article. Published on 18 February 2019. Downloaded on 1/26/2026 8:40:42 AM.
This article is licensed under a Creative Commons Attribution-NonCommercial 3.0 Unported Licence.

2. Experimental

2.1 Reagents

Palladium chloride ($PdCl_2$) and tetrachloroauric(III) acid ($HAuCl_4 \cdot 4H_2O$) were purchased from Sinopharm Chemical Reagent Co., Ltd. (Shanghai, China). Nessler's reagent and potassium sodium tartrate solution were purchased from Hefei Enfan Instrument Equipment Co., Ltd. (Hefei, China). All other chemicals were all of analytical grade. Ultrapure water (Millipore, 18.25 MΩ cm, Ulupure Science and Technology Co., Ltd., Chengdu, China) was used for the solution preparation. All chemicals were used as received without further purification.

2.2 Preparation of the catalysts

AuPd NPs with different Au-to-Pd ratios supported on Vulcan XC-72 carbon black were prepared using a facile impregnation-$NaBH_4$ reduction method without the addition of any stabilizer.[45] For the preparation of Au_3Pd_1/C catalyst, 108.0 mg of Vulcan XC-72 carbon black was dispersed in 200 mL of H_2O with ultrasonication for 1 h. Then, a solution containing 0.9 mmol of $HAuCl_4$ and 0.3 mmol of H_2PdCl_4 was added into the Vulcan XC-72 carbon black suspension. Subsequently, 150 mL of a freshly prepared 0.16 mol L^{-1} $NaBH_4$ solution was dripped into the suspension under strong stirring. After stirring for another 8 h at 30 °C, the Au_3Pd_1/C catalyst was filtered, washed with ultrapure water, and dried under vacuum at 25 °C overnight. The catalysts with different Au-to-Pd molar ratios of 0.5 : 1, 1 : 1, 2 : 1, 4 : 1 and 5 : 1 were prepared following the same procedure using different amounts of $PdCl_2$ and $HAuCl_4$. For comparison, Pd/C and Au/C catalysts were also made. The total amount of metals in each catalyst was kept constant at 1.2 mmol.

2.3 Characterization

The morphologies of the AuPd/C catalysts were characterized using a JEM-1011 transmission electron microscope (TEM, JEOL, Japan). The crystallographic information of the AuPd/C catalysts was collected using a D8 Advance X-ray diffractometer (XRD, Bruker, Germany) and a JEM-2100 high-resolution transmission electron microscope (HRTEM, JEOL, Japan), respectively. The elemental composition of the catalyst was determined with an INCA Sight X energy-dispersive spectroscope (EDX, Oxford, USA). The XPS spectra were taken with an ESCALAB 250 X-ray photoelectron spectroscope (XPS, Thermo Fisher SCIENTIFIC, UK) equipped with an Al-Kα excitation source. The Au/Pd molar ratio was analyzed with an Agilent 5110 inductively coupled plasma-optical emission spectrometer (ICP-OES, Agilent Technologies, US).

2.4 Catalytic performance of the catalysts

A two-necked round-bottomed flask placed in an oil bath with a magnetic stirrer was used as the reactor. One neck of the flask was connected to a spherical condenser and then to a series of wash bottles containing 2.5 mol L^{-1} CuCl solution and 8 mol L^{-1} NaOH solution for the removal of CO and CO_2, respectively. After purification, the hydrogen generated from the flask was gathered in a gas burette. Prior to the reaction, 60 mg of AuPd/C catalyst was put in the flask, heated to a pre-set temperature and maintained at that temperature for 30 min to reach thermal equilibrium. The reaction was initiated by adding 10 mL solution containing 3 mol L^{-1} of FA and 3 mol L^{-1} of AF at 365 K through a constant-pressure dropping funnel connected to the other neck of the flask. The volume of hydrogen released from the reactor was monitored using the gas burette.

2.5 Kinetic study of the dehydrogenation

The effect of the FA–AF total concentration on the dehydrogenation was evaluated over 60 mg of Au_3Pd_1/C catalyst using 0.02 mol of FA–AF mixture with the same molar fraction of FA (x_{FA}) = 0.5 but different solution volumes. To determine the AF reaction order, a series of tests were performed over 60 mg of catalyst in 5 mL of FA–AF mixture with 5 mol L^{-1} FA and AF of different concentrations (1–7.5 mol L^{-1}) at 365 K. The reaction order of FA was determined by performing several tests in 5 mL FA–AF mixture with 5 mol L^{-1} AF and FA with concentration varying from 1 mol L^{-1} to 5 mol L^{-1}. The apparent activation energy of the dehydrogenation was determined over 60 mg of AuPd/C catalyst at different temperatures from 325 K to 365 K with a temperature increment of 10 K.

2.6 Stability of the catalyst

After each run of dehydrogenation, the catalyst was filtered from the FA–AF mixture, washed with ultrapure water and dried under vacuum at 298 K overnight. Then, the recovered catalyst was used for the subsequent runs.

2.7 Purity of hydrogen

Because CO and NH_3 may produce due to the dehydration of FA and the hydrolysis of AF, the purity of the hydrogen generated from the FA–AF mixture was analyzed. The CO content was analyzed using GC-7920 (GC, Beijing Zhongjiao Jinyuan Technology Co., Ltd., China) with thermal conductivity detector (TCD) and flame ionization detector (FID)-Methanator (detection limit: ∼5 ppm for CO). The NH_3 content at different temperatures was monitored with an EFD-NH precision ammonia-nitrogen analyzer (Hefei Enfan Instrument Equipment Co., Ltd., China) using Nessler's reagent spectrophotometry (l = 420 nm). The NH_3 detection limit is 0.02 mg L^{-1} (calculated by N). The instrument error is £±5%. The total volume ($V_{H_2+CO_2}$) of CO_2 and H_2 was recorded after removal of NH_3 with dilute H_2SO_4 solution. For further determination, the solution containing NH_4^+ was diluted to 25 mL with dilute H_2SO_4 solution.

3. Results and discussion

3.1 Structure and morphology of the catalyst

According to the TEM images of the newly prepared AuPd/C catalysts with different Au-to-Pd ratios shown in Fig. 1(A) and S1,† the mean particle sizes of $Au_{0.5}Pd_1$/C, Au_1Pd_1/C, Au_2Pd_1/C, Au_3Pd_1, Au_4Pd_1/C and Au_5Pd_1/C catalysts were 4.86, 4.29, 4.25, 4.18, 4.78 and 5.33 nm, respectively. The Au_3Pd_1 NPs with the

Open Access Article. Published on 18 February 2019. Downloaded on 1/26/2026 8:40:42 AM.
This article is licensed under a Creative Commons Attribution-NonCommercial 3.0 Unported Licence.

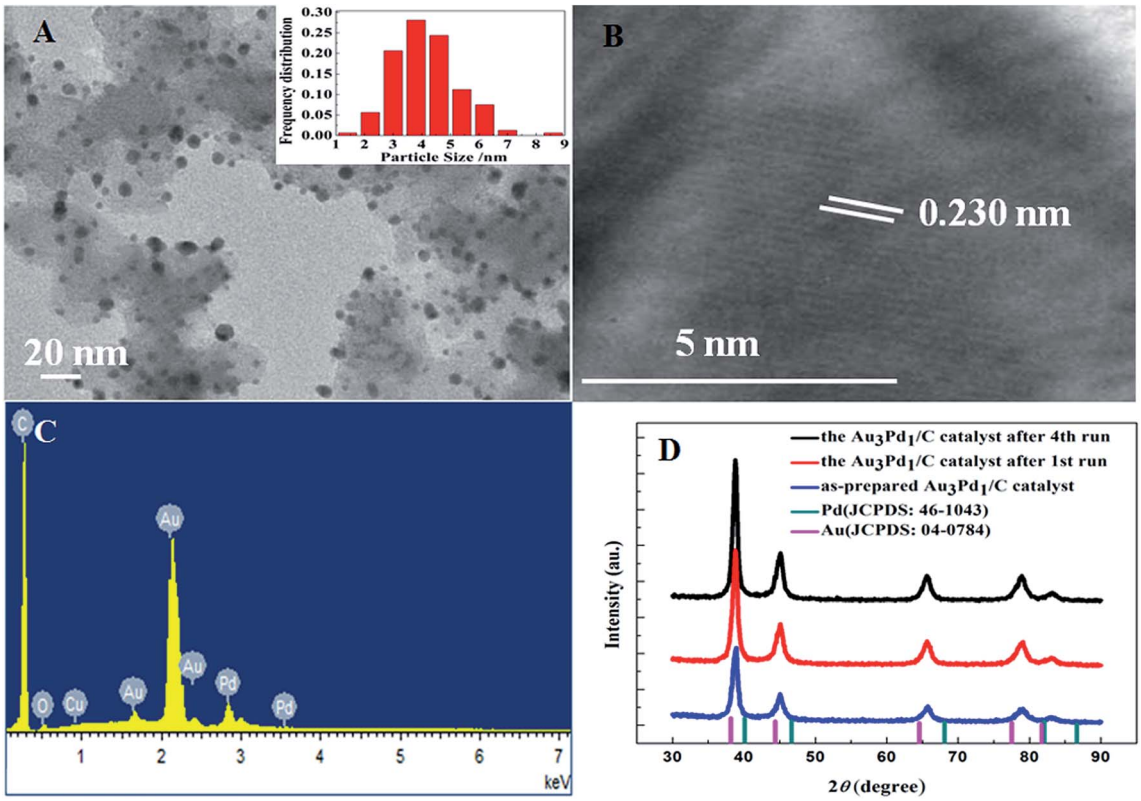

Fig. 1 (A) TEM image with the particle size distribution, (B) HR-TEM image, and (C) EDX spectrum of the newly prepared Au_3Pd_1/C catalyst. (D) XRD patterns of the newly prepared and recovered Au_3Pd_1/C catalysts after different experimental runs.

least particle size were uniformly distributed on the carbon support. According to the HR-TEM image shown in Fig. 1(B), a face-centred cubic (fcc) structure with a (111) facet lattice spacing of 0.230 nm can be observed. This lattice spacing is between the (111) spacing of fcc Au (0.236 nm, JCPDS file: 04-0784) and that of fcc Pd (0.225 nm, JCPDS file: 46-1043), suggesting the formation of AuPd alloy. The EDX spectrum shown in Fig. 1(C) shows the presence of both Au and Pd in the catalyst. The ICP-OES results of each catalysts are shown in Table S1.† The discrepancy between the expected AuPd composition and the confirmed composition in the resultant catalysts is small. According to Fig. 2, the characteristic diffraction peaks in the XRD patterns appear at a position between the Au and Pd peaks, which also suggests the formation of AuPd alloy.[40,45] Meanwhile, the position of the diffraction peaks shifts towards lower angles as the Au/Pd ratio increases, which is beneficial for electron transfer from Au to Pd.[52]

The binding energies of 83.71 eV, 87.36 eV, 84.70 eV, and 88.18 eV in the high-resolution Au 4f XPS (Fig. S4(B)†) spectrum correspond to Au^0 $4f_{7/2}$, Au^0 $4f_{5/2}$, Au^+ $4f_{7/2}$, and Au^+ $4f_{5/2}$, respectively. The binding energy of Au $4d_{5/2}$ (335 eV) is close to that of Pd $3d_{5/2}$ (335.1 eV),[53] which leads to the difficulty to separate the peak of Au $4d_{5/2}$ from the high-resolution XPS spectrum of Pd 3d (Fig. S4(C)†). The chemical states of Pd are Pd^0 (Pd $3d_{5/2}$, 334.50 eV; Pd $3d_{3/2}$, 340.15 eV), Pd^{2+} (Pd $3d_{5/2}$, 336.55 eV, Pd $3d_{3/2}$, 341.10 eV), and Pd^{4+} (Pd $3d_{5/2}$, 338.30 eV; Pd $3d_{3/2}$, 342.80 eV).[54,55] From the XPS results shown in Fig. 3, compared to Pd/C catalyst, it can be seen that a negative shift of the binding energy of Pd 3d in all AuPd/C catalysts, suggesting that Au may act as a cocatalyst which adjusts the electronic properties of Pd, consistent with the previous reports.[43,54,56] Moreover, the difference of the work functions of Pd (5.67 eV) and Au (5.54 eV) could also lead to the electron transfer from Au to Pd in AuPd alloy.[57] The low activity of single Au/C catalyst

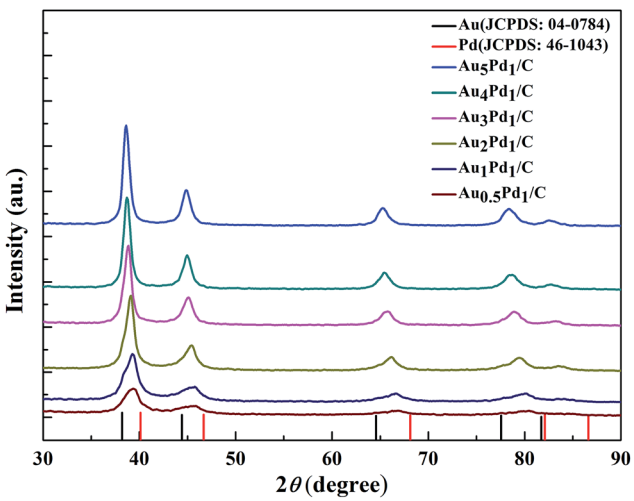

Fig. 2 XRD patterns of the newly prepared AuPd/C catalysts with different Au/Pd molar ratios.

Open Access Article. Published on 18 February 2019. Downloaded on 1/26/2026 8:40:42 AM.
This article is licensed under a Creative Commons Attribution-NonCommercial 3.0 Unported Licence.

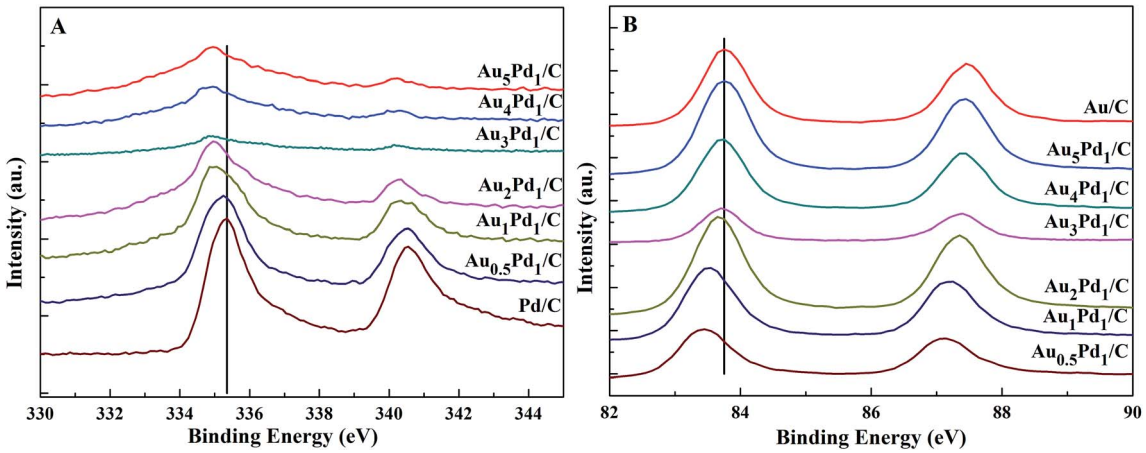

Fig. 3 High-resolution XPS spectra of (A) Pd 3d and (B) Au 4f in the newly prepared AuPd/C catalysts with different Au/Pd molar ratios.

shown in Fig. S3† also backs up this conclusion. The reduced binding energy of Pd in AuPd catalyst reduces the interaction between Pd surface and CO or H atoms,[35,39,56] which is beneficial for the stability of the catalyst as revealed in Fig. S3.† The surface composition of the AuPd catalyst was characterized using XPS. According to the XPS results shown in Table S2,† the surface Au content is less than the overall content, suggesting surface enrichment of Pd in the AuPd catalysts.

3.2 Effect of catalyst composition

According to the catalytic performances of Pd/C, Au/C and Au_3Pd_1/C catalysts in the FA–AF mixture shown in Fig. S3,† both the catalytic activity and stability of the Au_3Pd_1/C catalyst is much better than that of the Pd/C and Au/C catalysts. The dehydrogenation rate of the Pd/C catalyst is fast at beginning but slows down rapidly, suggesting poor stability.

The effect of the Au–Pd molar ratio on the dehydrogenation and the dependence of initial TOF on the molar ratio of Au–Pd are shown in Fig. 4. The Au–Pd molar ratio has a significant effect on the catalytic activity with the optimal composition of Au_3Pd_1. Therefore, the Au_3Pd_1/C catalyst was chosen for further study.

For the Au_3Pd_1/C catalyst, the H_2 volume can reach 750 mL after 3 h of reaction, corresponding to an initial TOF for the first 1 h of 99.2 h^{-1}. 750 mL of H_2 corresponds to the complete dehydrogenation of FA and 11.6% dehydrogenation of AF.[51]

3.3 Kinetic and mechanism study

As shown in Fig. 5, the initial rate of dehydrogenation increases with increasing the total FA–AF concentration, while the maximum hydrogen volume does not change significantly. The complete decomposition of FA and 37.1–47.3% decomposition of AF were observed. The detail information is given in Table S3.†

According to Fig. 6(A), the dehydrogenation rate significantly increases with an increasing concentration of AF. In Fig. 6(B), there is a linear relationship between the logarithm of the initial TOF for the first 10 min and AF concentration with a slope of 0.55 and a linear correlation coefficient, $R^2 = 0.99$. Therefore, the reaction order with respect to AF is 0.55. Similarly,

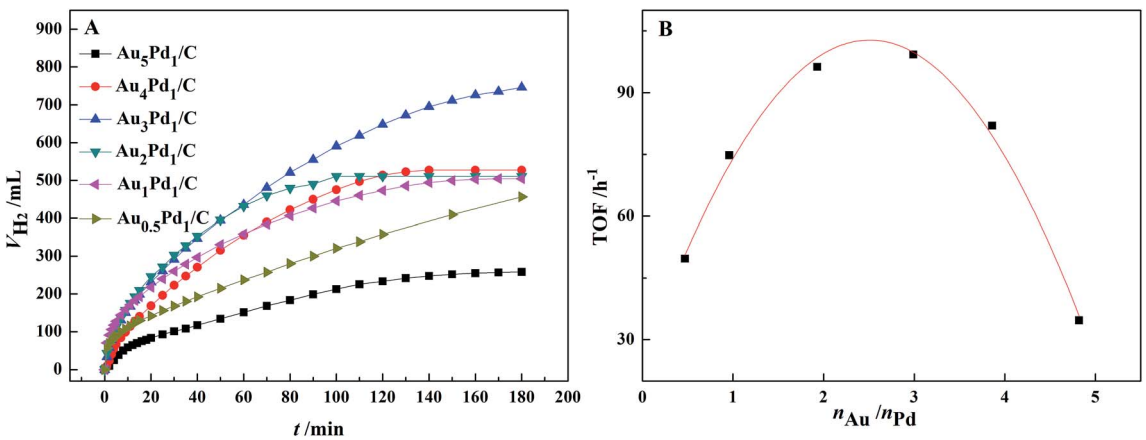

Fig. 4 (A) Effect of the Au–Pd molar ratio on the dehydrogenation of 10 mL FA–AF mixture with 3 mol L^{-1} FA and 3 mol L^{-1} AF at 365 K; (B) the dependence of initial TOF on the Au–Pd molar ratio.

Open Access Article. Published on 18 February 2019. Downloaded on 1/26/2026 8:40:42 AM.
This article is licensed under a Creative Commons Attribution-NonCommercial 3.0 Unported Licence.

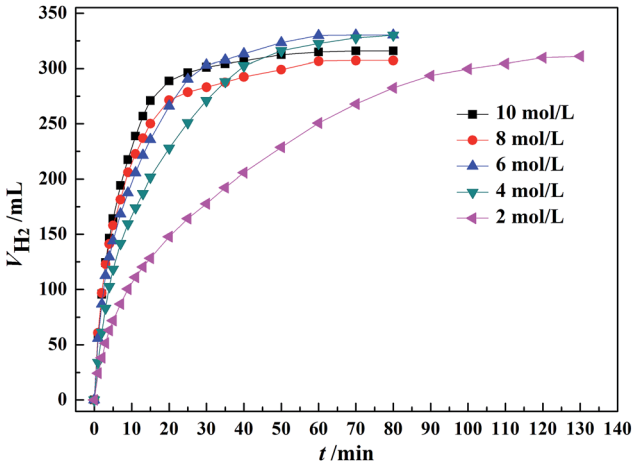

Fig. 5 Effect of the total concentration of FA–AF mixture on the H_2 generation over 60 mg of Au_3Pd_1/C catalyst from FA–AF mixtures with 0.01 mol FA and 0.01 mol AF at 365 K.

according to Fig. 6(D), a reaction order with respect to FA is 0.25. The rate equation for the dehydrogenation of FA–AF mixture over Au_3Pd_1/C catalyst is:

$$r = k[\mathrm{HCOOH}]^{0.25}[\mathrm{HCOONH_4}]^{0.55} \quad (3)$$

Eqn (3) suggests that the dehydrogenation rate of FA–AF mixture over Au_3Pd_1/C catalyst is more sensitive to the AF concentration. The fractional reaction orders of FA and AF suggest that the mechanism of dehydrogenation of the FA–AF mixture is complicated. The higher partial reaction order of AF in eqn (3) may be ascribed to three cases. For Case I, the $HCOO^-$ with a rather higher concentration is a reactive intermediate,[46,58] and the existence of $HCOO^-$ is conducive for FA to form a "H-down" adsorption configuration on the catalyst surface,[59,60] beneficial for the dehydrogenation of FA. For Case II, $HCOO^-$ forms an equilibrium with HCOOH:

$$\mathrm{HCOOH} \rightleftharpoons \mathrm{HCOO^-} + \mathrm{H^+} \quad (4)$$

Once FA is consumed, the equilibrium shifts left and replenishes FA, contradicting the decrease in the reactant concentration and reaction rate. For Case III, AF decomposes over the catalyst with a higher rate.

For Case I, AF does not take part in the reaction; for Case II, a linear response with the same reaction order as that of FA should be observed, which is not consistent with the experimental results; for Case III, AF with a higher dehydrogenation activity can indeed exhibit a higher reaction order.

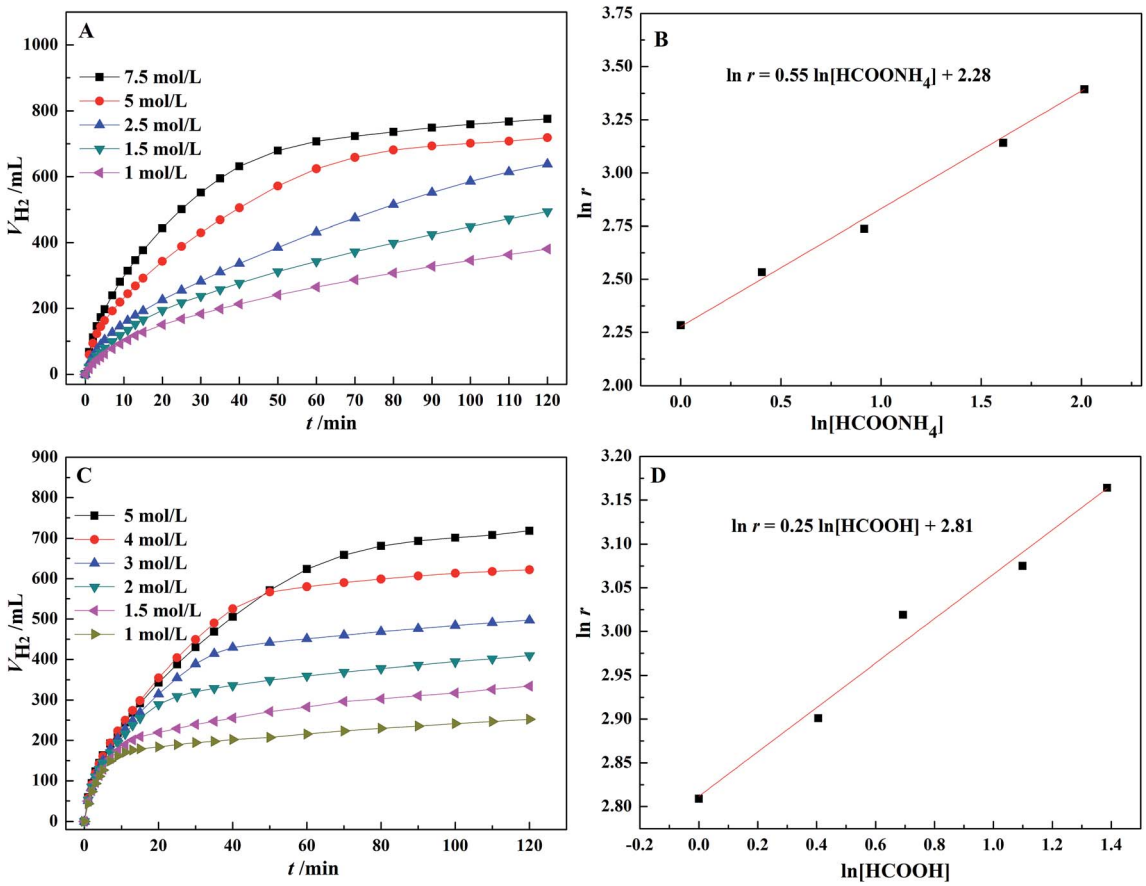

Fig. 6 (A) The effect of AF concentration on the H_2 generation from 5 mL FA–AF mixture containing 5 mol L^{-1} FA; (B) the logarithm of reaction rate *vs.* AF concentration; (C) the effect of FA concentration on the H_2 generation from 5 mL FA–AF mixture containing 5 mol L^{-1} AF; (D) the logarithm of reaction rate *vs.* FA concentration. The experiments were conducted over 60 mg of Au_3Pd_1/C catalyst at 365 K.

Open Access Article. Published on 18 February 2019. Downloaded on 1/26/2026 8:40:42 AM.
This article is licensed under a Creative Commons Attribution-NonCommercial 3.0 Unported Licence.

For Case III, AF decomposes following eqn (5):

$$HCOO^- + H_2O \xrightarrow{cat} HCO_3^- + H_2\uparrow \quad (5)$$

HCO_3^- can react with concentrated FA according to eqn (6):

$$HCO_3^- + HCOOH \xrightarrow{cat} HCOO^- + H_2O + CO_2\uparrow \quad (6)$$

Thus, the overall reaction for dehydrogenation of FA can be written as:[61]

$$HCOOH \xrightarrow{cat} H_2\uparrow + CO_2\uparrow \quad (7)$$

Eqn (7) suggests that, when there is sufficient FA, AF will not decompose. In other words, in FA–AF mixture, FA will decompose first with AF serving as a catalyst.

When FA is completely consumed, AF begins to decompose through the following reactions:[62]

$$HCOONH_4 \rightarrow HCOO^- + NH_4^+ \quad (8)$$

$$HCOO^- + H_2O \xrightarrow{cat} HCO_3^- + H_2\uparrow \quad (9)$$

$$HCO_3^- + NH_4^+ \rightleftharpoons H_2O + NH_3\uparrow + CO_2\uparrow \quad (10)$$

Eqn (10) is a double hydrolysis reaction with the hydrolysis of HCO_3^- and NH_4^+ enhancing each other. At this moment, the overall reaction is

$$HCOONH_4 \xrightarrow{cat} NH_3\uparrow + H_2\uparrow + CO_2\uparrow \quad (11)$$

For FA–AF system with a high concentration of FA, H^+ is plentiful such that the supply of H^+ does not depend on the hydrolysis of NH_4^+.[50] The presence of a high concentration of FA can block the direct dehydrogenation of AF. However, if the reaction rate of eqn (9) is not fast enough, there is a possibility for the FA–AF system to sent off NH_3 which is harmful for the further application of hydrogen. NH_3 as a possible contaminant should be concerned.

According to Fig. 7(A), the initial dehydrogenation rate increases with increasing reaction temperature. The FA–AF mixture with 5 mol L^{-1} FA and 7.5 mol L^{-1} AF offers the highest initial TOF of for the first 10 min of 407.5 h^{-1} over the Au_3Pd_1/C catalyst at 365 K. The increased dehydrogenation activity of FA over the AuPd-based catalysts can also be confirmed.[36,45] According to Fig. 7(B), the apparent activation energy was 23.3 ± 1.3 kJ mol^{-1}, lower than that of some previous reports (Table S4†). On the other hand, the AuPd/C catalyst used in this study is prepared without addition of any stabilizer, and the preparation procedure is more producible and facial than that reported elsewhere.

3.4 Stability of the catalyst

The stability of the catalyst was investigated by using the recovered Au_3Pd_1/C for subsequent dehydrogenation runs. According to Fig. 8, the maximum H_2 volume produced over the newly prepared Au_3Pd_1/C catalyst was 856.0 mL. For the 2nd, 3rd and 4th run, the maximum H_2 volumes produced over the recovered Au_3Pd_1/C catalysts were 786.3 mL, 704.0 mL, and 769.5 mL, respectively. Therefore, the maximum H_2 volume for the 4th run remains *ca.* 88.0% of the first run. This result suggests that the stability of the Au_3Pd_1/C catalyst is much better than that of the single Pd/C catalyst as we expected.[51]

In Fig. S2,† according to the TEM images and the particle size distribution, the mean particle size of the recovered Au_3Pd_1 NPs was 4.46 nm after the first run and 4.43 nm after the fourth run. This means the aggregation of the Au_3Pd_1 NPs during dehydrogenation is not obvious.

3.5 Purity of hydrogen

According to the above results, the FA–AF mixture with 5 mol L^{-1} FA and 7.5 mol L^{-1} AF over the Au_3Pd_1/C catalyst at 365 K is an appealing system with enhanced activity and improved stability for hydrogen generation. However, owing to reactions (2), (10) and (11), CO and NH_3 may possibly generate during dehydrogenation. These two contaminants are both harmful to the Pt catalyst used in hydrogen–oxygen fuel cell. It

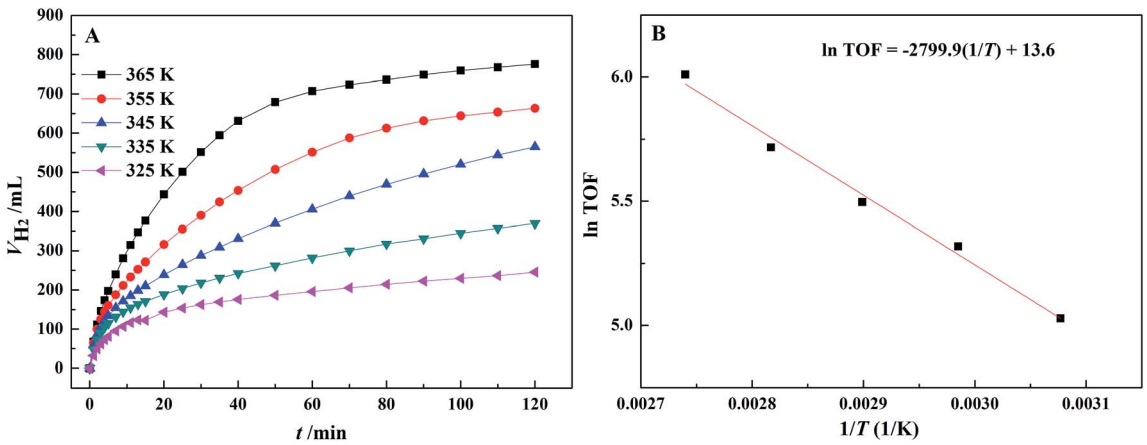

Fig. 7 (A) Effect of temperature on the dehydrogenation of 5 mL FA–AF mixture containing 5 mol L^{-1} FA and 7.5 mol L^{-1} AF over the Au_3Pd_1/C catalyst; (B) Arrhenius plot of the dehydrogenation.

Open Access Article. Published on 18 February 2019. Downloaded on 1/26/2026 8:40:42 AM.
This article is licensed under a Creative Commons Attribution-NonCommercial 3.0 Unported Licence.

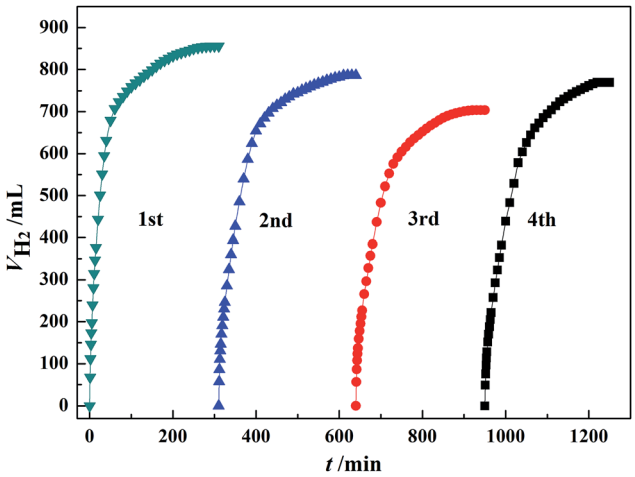

Fig. 8 Dehydrogenation of 5 mL FA–AF mixture containing 5 mol L^{-1} FA and 7.5 mol L^{-1} AF over 60 mg of newly prepared and recovered Au_3Pd_1/C catalysts at 365 K.

was found that even the content of NH_3 is as low as 1 ppm, it can significantly deteriorate the performance of the proton exchange membrane fuel cells (PEMFC).[63–65] Therefore, the content of CO and NH_3 in hydrogen was both monitored.

According to the results shown in Fig. S5 and S6,† the content of CO is less than the detection limit (*ca.* 5 ppm). This means that the production of CO is not obvious for our new system. According to Fig. S7,† the content of NH_3 changes with temperature. At 365 K, the NH_3 content is very high due to the enhanced double hydrolysis as shown in eqn (10) and the reduced solubility of NH_3 in water. If we reduced the reaction temperature, the NH_3 content in hydrogen reduced significantly. However, even if the reaction temperature is reduced to 325 K, the NH_3 content still remains at 29.6 ± 4.6 ppm, which is still higher than the permitted value. This is can be attributed to the small rate of eqn (6). If we want to use FA–AF mixture and Au_3Pd_1/C catalyst for hydrogen production, more effort should be made to accelerate eqn (6) and reduce reaction temperature without obvious lowering of the catalytic activity.

4. Conclusions

Compared to the single Pd/C catalyst, the Au_3Pd_1/C catalyst exhibits improved activity and stability towards the dehydrogenation of FA–AF mixture. The reaction order with respect to AF and FA is 0.55 and 0.25, respectively. The dehydrogenation mechanism for FA–AF mixture is complicated. AF acts as a catalyst for the dehydrogenation of FA and can also undergo dehydrogenation even if FA is enough. Further effort should be made to reduce the NH_3 content before the FA–AF mixture with Au_3Pd_1 NPs serving as catalyst can be used as promising hydrogen storage materials.

Conflicts of interest

There are no conflicts to declare.

Acknowledgements

This work was financially supported by the Shandong Self Innovation project (No. 012CX80106).

Notes and references

1 A. Züttel, A. Remhof, A. Borgschulte and O. Friedrichs, *Philos. Trans. R. Soc., A*, 2010, **368**, 3329–3342.
2 E. S. Hanley, J. P. Deane and B. P. Ó. Gallachóir, *Renewable Sustainable Energy Rev.*, 2018, **82**, 3027–3045.
3 P. P. Edwards, V. L. Kuznetsov, W. I. F. David and N. P. Brandon, *Energy Policy*, 2008, **36**, 4356–4362.
4 M. Balat, *Int. J. Hydrogen Energy*, 2008, **33**, 4013–4029.
5 N. Muradov and T. Veziroglu, *Int. J. Hydrogen Energy*, 2008, **33**, 6804–6839.
6 A. F. Dalebrook, W. Gan, M. Grasemann, S. Moret and G. Laurenczy, *Chem. Commun.*, 2013, **49**, 8735–8751.
7 M. Felderhoff, C. Weidenthaler, R. von Helmolt and U. Eberle, *Phys. Chem. Chem. Phys.*, 2007, **9**, 2643–2653.
8 A. W. C. van den Berg and C. O. Areán, *Chem. Commun.*, 2008, 668–681.
9 M. Nielsen, A. Kammer, D. Cozzula, H. Junge, S. Gladiali and M. Beller, *Angew. Chem., Int. Ed.*, 2011, **50**, 9593–9597.
10 T. C. Johnson, D. J. Morris and M. Wills, *Chem. Soc. Rev.*, 2010, **39**, 81–88.
11 S. Enthaler, J. von Langermann and T. Schmidt, *Energy Environ. Sci.*, 2010, **3**, 1207–1217.
12 H. L. Jiang, S. K. Singh, J. M. Yan, X. B. Zhang and Q. Xu, *ChemSusChem*, 2010, **3**, 541–549.
13 B. Loges, A. Boddien, F. Gärtner, H. Junge and M. Beller, *Top. Catal.*, 2010, **53**, 902–914.
14 K. Mandal, D. Bhattacharjee and S. Dasgupta, *Int. J. Hydrogen Energy*, 2015, **40**, 4786–4793.
15 M. Grasemann and G. Laurenczy, *Energy Environ. Sci.*, 2012, **5**, 8171–8181.
16 Y. Zhu, Y. Kang, Z. Zou, Q. Zhou, J. Zheng, B. Xia and H. Yang, *Fuel Cells Bulletin*, 2008, **2008**, 12–15.
17 J. J. Baschuk and X. G. Li, *Int. J. Energy Res.*, 2001, **25**, 695–713.
18 W. Wang, W. Wang and S. Chen, *Int. J. Hydrogen Energy*, 2016, **41**, 20680–20692.
19 K. Tedsree, T. Li, S. Jones, C. W. Chan, K. M. Yu, P. A. Bagot, E. A. Marquis, G. D. Smith and S. C. Tsang, *Nat. Nanotechnol.*, 2011, **6**, 302–307.
20 Z. Z. Wang, H. Y. Zhang, L. Li, S. S. Miao, S. J. Wu, X. F. Hao, W. X. Zhang and M. J. Jia, *Catal. Commun.*, 2018, **114**, 51–55.
21 S. Q. Zhang, Y. R. Lee, H. J. Jeon, W. S. Ahn and Y. M. Chung, *Mater. Lett.*, 2018, **215**, 211–213.
22 M. Navlani-García, D. Salinas-Torres, K. Mori, A. F. Léonard, Y. Kuwahara, N. Job and H. Yamashita, *Catal. Today*, 2019, **324**, 90–96.
23 Q. Y. Bi, J. D. Lin, Y. M. Liu, H. Y. He, F. Q. Huang and Y. Cao, *Angew. Chem., Int. Ed.*, 2016, **55**, 11849–11853.
24 Q. L. Zhu, N. Tsumori and Q. Xu, *J. Am. Chem. Soc.*, 2015, **137**, 11743–11748.

Open Access Article. Published on 18 February 2019. Downloaded on 1/26/2026 8:40:42 AM.
This article is licensed under a Creative Commons Attribution-NonCommercial 3.0 Unported Licence.

25 M. Yadav, A. K. Singh, N. Tsumori and Q. Xu, *J. Mater. Chem.*, 2012, **22**, 19146–19150.
26 S. Akbayrak, Y. Tonbul and S. Özkar, *Appl. Catal., B*, 2017, **206**, 384–392.
27 Y. Q. Chen, X. F. Li, Z. Z. Wei, S. J. Mao, J. Deng, Y. L. Cao and Y. Wang, *Catal. Commun.*, 2018, **108**, 55–58.
28 Q. Y. Bi, J. D. Lin, Y. M. Liu, F. Q. Huang and Y. Cao, *Int. J. Hydrogen Energy*, 2016, **41**, 21193–21202.
29 Q. G. Liu, X. F. Yang, Y. Q. Huang, S. T. Xu, X. Su, X. L. Pan, J. M. Xu, A. Q. Wang, C. H. Liang, X. K. Wang and T. Zhang, *Energy Environ. Sci.*, 2015, **8**, 3204–3207.
30 D. A. Bulushev, M. Zacharska, Y. N. Guo, S. Beloshapkin and A. Simakov, *Catal. Commun.*, 2017, **92**, 86–89.
31 M. Ojeda and E. Iglesia, *Angew. Chem., Int. Ed.*, 2009, **48**, 4800–4803.
32 M. Yadav, T. Akita, N. Tsumori and Q. Xu, *J. Mater. Chem.*, 2012, **22**, 12582–12586.
33 Q. Y. Bi, J. D. Lin, Y. M. Liu, H. Y. He, F. Q. Huang and Y. Cao, *J. Power Sources*, 2016, **328**, 463–471.
34 R. H. Li, X. H. Zhu, X. Q. Yan, D. H. Shou, X. Zhou and W. X. Chen, *RSC Adv.*, 2016, **6**, 100103–100107.
35 F. Abild-Pedersen and M. P. Andersson, *Surf. Sci.*, 2007, **601**, 1747–1753.
36 X. Zhou, Y. Huang, W. Xing, C. Liu, J. Liao and T. Lu, *Chem. Commun.*, 2008, 3540–3542.
37 W. Y. Yu, G. M. Mullen and C. B. Mullins, *J. Phys. Chem. C*, 2013, **117**, 19535–19543.
38 S. Singh, S. Li, R. Carrasquillo-Flores, A. C. Alba-Rubio, J. A. Dumesic and M. Mavrikakis, *AIChE J.*, 2014, **60**, 1303–1319.
39 D. Liu, Z. Y. Gao, X. C. Wang, J. Zeng and Y. M. Li, *Appl. Surf. Sci.*, 2017, **426**, 194–205.
40 L. X. Xu, F. Yao, J. L. Luo, C. Wan, M. F. Ye, P. Cui and Y. An, *RSC Adv.*, 2017, **7**, 4746–4752.
41 Y. L. Qin, J. W. Wang, Y. M. Wu and L. M. Wang, *RSC Adv.*, 2014, **4**, 30068–30073.
42 S. Wu, F. Yang, P. C. Sun and T. H. Chen, *RSC Adv.*, 2014, **4**, 44500–44503.
43 Y. Q. Jiang, X. L. Fan, X. Z. Xiao, X. Huang, M. J. Liu, S. Q. Li, H. W. Ge and L. X. Chen, *Int. J. Hydrogen Energy*, 2017, **42**, 9353–9360.
44 X. Gu, Z. H. Lu, H. L. Jiang, T. Akita and Q. Xu, *J. Am. Chem. Soc.*, 2011, **133**, 11822–11825.
45 Y. J. Huang, X. C. Zhou, M. Yin, C. P. Liu and W. Xing, *Chem. Mater.*, 2010, **22**, 5122–5128.
46 J. Guo, Y. Y. Gao, C. H. Tan, Y. P. Li, S. L. Zhao, L. Z. Bai and S. Y. Zhang, *Fuel Cells*, 2013, **13**, 167–172.
47 K. Jiang, K. Xu, S. Zou and W. B. Cai, *J. Am. Chem. Soc.*, 2014, **136**, 4861–4864.
48 L. Yang, X. Hua, J. Su, W. Luo, S. L. Chen and G. Z. Cheng, *Appl. Catal., B*, 2015, **168–169**, 423–428.
49 L. Yang, W. Luo and G. Z. Cheng, *Int. J. Hydrogen Energy*, 2016, **41**, 439–446.
50 J. Su, L. Yang, M. Lu and H. Lin, *ChemSusChem*, 2015, **8**, 813–816.
51 J. P. Zhou, J. Zhang, X. H. Dai, X. Wang and S. Y. Zhang, *Int. J. Hydrogen Energy*, 2016, **41**, 22059–22066.
52 P. Liu, X. Gu, H. Zhang, J. Cheng, J. Song and H. Su, *Appl. Catal., B*, 2017, **204**, 497–504.
53 *NIST XPS Database*, http://srdata.nist.gov/xps/selEnergyType.aspx, accessed September 2012.
54 Z. L. Wang, J. M. Yan, H. L. Wang, Y. Ping and Q. Jiang, *J. Mater. Chem. A*, 2013, **1**, 12721–12725.
55 Z. Y. Zhang, S. W. Cao, Y. S. Liao and C. Xue, *Appl. Catal., B*, 2015, **62**, 204–209.
56 X. Zhou, Y. Huang, C. Liu, J. Liao, T. Lu and W. Xing, *ChemSusChem*, 2010, **3**, 1379–1382.
57 Z. L. Wang, J. M. Yan, Y. Ping, H. L. Wang, W. T. Zheng and Q. Jiang, *Angew. Chem.*, 2013, **125**, 4502–4505.
58 J. Joo, T. Uchida, A. Cuesta, M. T. Koper and M. Osawa, *J. Am. Chem. Soc.*, 2013, **135**, 9991–9994.
59 B. Peng, H. F. Wang, Z. P. Liu and W. B. Cai, *J. Phys. Chem. C*, 2010, **114**, 3102–3107.
60 H. F. Wang and Z. P. Liu, *J. Phys. Chem. C*, 2009, **113**, 17502–17508.
61 X. Wang, G. W. Qi, C. H. Tan, Y. P. Li, J. Guo, X. J. Pang and S. Y. Zhang, *Int. J. Hydrogen Energy*, 2014, **39**, 837–843.
62 M. A. Tike and V. V. Mahajani, *Chem. Eng. J.*, 2006, **123**, 31–41.
63 R. Halseid, P. J. S. Vie and R. Tunold, *J. Power Sources*, 2006, **154**, 343–350.
64 F. A. Uribe, S. Gottesfeld and T. A. Zawodzinski, *J. Electrochem. Soc.*, 2002, **149**, A293–A296.
65 H. J. Soto, W. K. Lee, J. W. Van Zee and M. Murthy, *Electrochem. Solid-State Lett.*, 2003, **6**, A133–A135.

 This journal is © The Royal Society of Chemistry 2019